

# A Passive LC Filter Based Harmonic Compensation for Multilevel Cascaded Inverters under Unbalanced Dc Sources Using NVM Control Technique

T.Manohar Reddy<sup>1</sup>, B.Yella Reddy<sup>2</sup>

<sup>1</sup>M.Tech, Scholar, Dept. of EEE, Newton's Institute of Engineering, Macherla  
<sup>2</sup>assistant Professor, Dept. of EEE, Newton's Institute of Engineering, Macherla

**Abstract-** This paper proposes passive lc filter network based multilevel cascaded inverters with pulse width-modulation strategy to achieve balanced line-to-line output voltages and to maximize the modulation index in the linear modulation range where the output voltage can be linearly adjusted in the multilevel cascaded inverter (MLCI) operating under unbalanced dc-link conditions. A neutral voltage modulation strategy is proposed to achieve output voltage balancing as well as to extend the linear modulation range up to the maximum reachable point in theory. In the proposed method, too large of a dc-link imbalance precludes the balancing of the output voltages. The simulations for a seven-level phase-shifted modulated MLCI for electric vehicle traction motor drive show that the proposed method is able to balance line-to-line output voltages as well as to maximize the linear modulation range under the unbalanced dc-link conditions.

**Index Terms-** Harmonic injection, multilevel cascaded inverters (MLCIs), neutral voltage modulation (NVM), phase-shifted (PS) modulation, space vector pulse width modulation (PWM) (SVPWM).

## I. INTRODUCTION

Multilevel Inverters enable the synthesis of a sinusoidal output voltage from several steps of voltages. For this reason, multilevel inverters have low dv/dt characteristics and generally have low harmonics in the output voltage and current. In addition, the switching of very high voltages can be achieved by stacking multilevel inverter modules [1]–[5]. Due to these advantages, multilevel inverters have been applied in various application fields [6]. In MLCI applications, a Modulation strategy to generate gating signals is very crucial to achieve high-performance control. Regarding this issue, many studies have been conducted, and they are roughly

categorized into multilevel selective harmonic elimination pulse width modulation (PWM) (SHEPWM), multilevel carrier-based PWM, and multilevel space vector PWM (SVPWM) methods [4].

Generally, a carrier-based PWM or SVPWM is preferred in applications such as motor drives [15], where dynamic properties are very important, whereas SHEPWM is preferred in some high-power static power conversion applications. In an SVPWM method has been studied to cover the over modulation range in the multilevel inverter. To reduce the common-mode voltage, a multilevel SVPWM has been proposed. The series SVPWM method has been reported to easily implement SVPWM for the MLCI.

The performances of a carrier-based PWM and an SVPWM are compared, and a PWM scheme is proposed to obtain an optimal output voltage in the multilevel inverter. On the other hand, MLCIs require separated dc links. Therefore, if there is one or more faults present in the dc links in each phase, or if the voltage magnitudes of the dc links are unequal, the output voltage of the MLCI can be unbalanced without proper compensation. To resolve this issue, some studies have been conducted.

A neutral voltage shifting technique has been introduced for balancing the state of charge in the MLCI-based battery energy storage system. In duty cycle modification method has been proposed to compensate an output voltage imbalance caused by single-phase power fluctuations. Reference has shown that a zero sequence component helps to obtain the maximum balanced output voltages in a fault condition. An offset voltage injection technique is studied to balance the output voltage of the MLCI,

but the use of an integrator in the compensation method may reduce dynamic characteristics in applications such as EV motor drives.

In this paper, a carrier-based PWM strategy to balance line to line output voltages and to maximize the linear modulation range where the output voltage can be linearly controlled in the MLCI operating under unbalanced dc-link conditions is proposed. In unbalanced dc-link conditions, the maximum synthesizable voltage in each phase is not uniform. Consequently, the linear modulation range is reduced, and a significant output voltage imbalance may occur as output voltage references increase. In order to analyze the imbalance effect, the voltage vector space for the MLCI is evaluated in detail. From this analysis, the theory behind the output voltage imbalance is explained, and the maximum linear modulation range considering unbalanced dc sources is evaluated. After that, a neutral voltage modulation (NVM) strategy is proposed to achieve output voltage balancing as well as to extend the linear modulation range up to the maximum reachable point in theory.

In the proposed method, the neutral voltage reference, which considers a zero sequence voltage to compensate the output voltage imbalance, and an offset voltage to extend the linear modulation range are easily obtained through simple arithmetic calculations. In the proposed method, too large of a dc-link imbalance precludes the output voltages from being balanced.

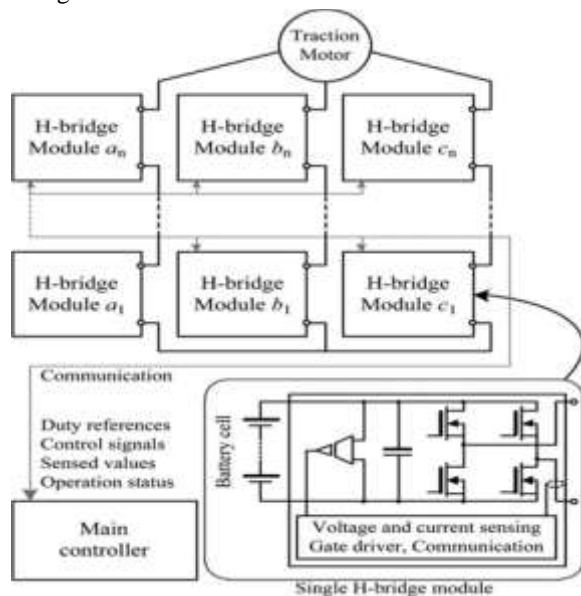


Fig.1. MLCI-based inverter for EV traction drive

## II. SYSTEM CONFIGURATION AND VOLTAGE VECTOR SPACE ANALYSIS

### A. Configuration of MLCI for EV Traction Motor Drive

Fig. 1 shows the EV traction motor drive system that is dealt within this paper. In this configuration, various power ratings can be easily implemented by configuring the number of the single H-bridge modules according to a required specification Such as a neighbourhood EV, full-size sedan, and so on. Here each H-bridge module incorporates voltage and current sensing circuitries, gate drivers, and communication interfaces between the module itself and the main controller. In addition, battery cells can be also included in the H-bridge module.

The unipolar modulation technique is applied between two switching legs in the H-bridge module. Consequently, the effective switching frequency in each H-bridge module is twice the carrier frequency. In addition to this, the well-known PS modulation technique is Used to implement interleaving and multilevel operation. Therefore, the effective switching frequency  $f_{sw}$  in a phase is where  $N$  and  $f_c$  represent the number of the H-bridge modules in each phase and the carrier frequency of PWM, respectively. As an example, Fig. 2 shows the carriers for each module, the duty cycles in unipolar modulation, and the output voltage When  $N = 2$ . B. Voltage Vector Space Analysis When the dc-link voltage of a single H-bridge module is  $V_{dc}$  the output voltage  $v_{pn}$  has three states, i.e.,  $V_{dc}$ ,  $0$ , and  $-V_{dc}$ ,

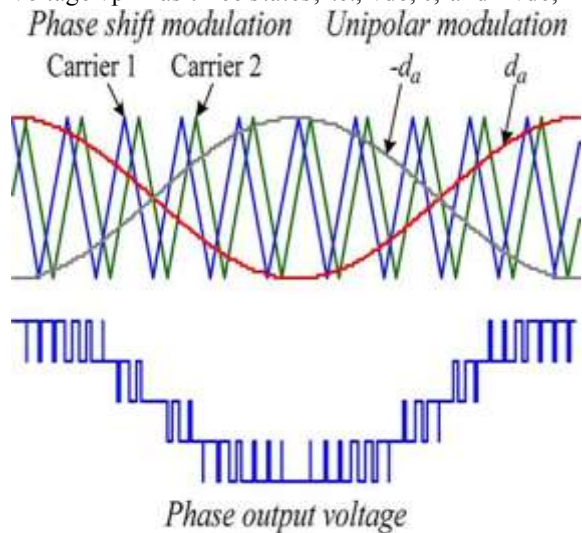


Fig. 2. Unipolar and phase shift modulation for single H-bridge module

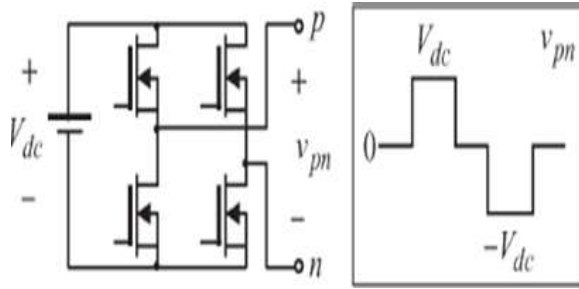


Fig.3. Output voltage of a single H-bridge module

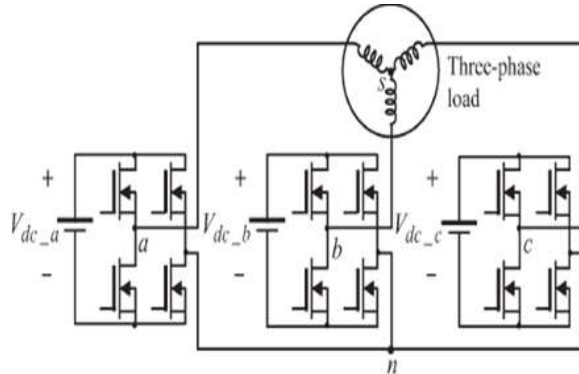


Fig.4. One-by-three configuration MLCI.

As shown in Fig. 3. By adopting the concept of a switching Function, it can be represented as

$$v_{pn} = S_p V_{dc}$$

$$S_p \in \{-1, 0, 1\}_{p=a,b,or,c} \quad (2)$$

Where  $S_p$  is a switching function and  $p$  can be replaced with  $a, b,$  or  $c,$  which represent the phases.

Fig. 4 shows a simple one-by-three configuration MLCI. For voltage vector space analysis, the main concept is derived from this simple topology, and then, it is expanded to more levels. In Fig. 4, there are two neutral points  $s$  and  $n$  in the MLCI. Here, the voltage between the output point of each phase and the neutral point  $n$  is defined as the pole voltage. The pole voltages are represented as  $v_{an}, v_{bn},$  and  $v_{cn}.$  The voltage between the output point of each phase and the load side neutral point  $s$  is Specified as the phase voltage. The phase voltages include  $v_{as}, v_{bs},$  and  $v_{cs}.$

By using this concept, the voltage between the two neutral points is defined as  $v_{sn}$  and can be written as

$$v_{sn} = -v_{as} + v_{an} = -v_{bs} + v_{bn} = -v_{cs} + v_{cn} \quad (3)$$

By using the condition that the sum of all phase voltages is zero because the load does not have a neutral line,  $v_{sn}$  is rewritten as

$$v_{sn} = \frac{1}{3}(v_{an} + v_{bn} + v_{cn}). \quad (4)$$

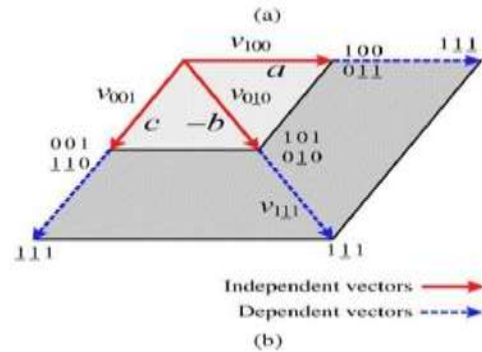
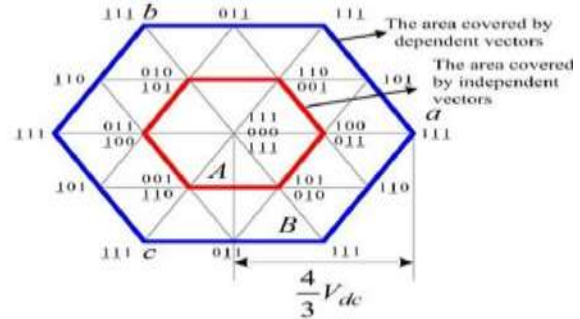


Fig.5. Voltage vector space of one-by-three configuration MLCI

By substituting (4) into (3), the phase voltage of each phase is represented as follows by using the relationship defined in (2):

$$v_{as} = \frac{2}{3}S_a V_{dc\_a} - \frac{1}{3}S_b V_{dc\_b} - \frac{1}{3}S_c V_{dc\_c}$$

$$v_{bs} = -\frac{1}{3}S_a V_{dc\_a} + \frac{2}{3}S_b V_{dc\_b} - \frac{1}{3}S_c V_{dc\_c}$$

$$v_{cs} = -\frac{1}{3}S_a V_{dc\_a} - \frac{1}{3}S_b V_{dc\_b} + \frac{2}{3}S_c V_{dc\_c} \quad (5)$$

If the magnitudes of three dc links are balanced so that  $V_{dc\_a}, V_{dc\_b},$  and  $V_{dc\_c}$  have the same value  $V_{dc},$  the voltage vector space in  $\alpha-\beta$  coordinates is defined in Fig. 5(a) by using (5). In the figure, underbars indicate that the switching function has the value of  $-1.$  A part of the hexagon in Fig. 5(a) is shown in Fig. 5(b). In this figure, the vectors  $v_{010}$  and  $v_{111}$  are placed at the same reference axis, phase  $b.$  However, the constituents of those vectors are different. For  $v_{010},$  this vector can be synthesized without the other two phases' assistance. However,  $v_{111}$  cannot be produced without other vectors according to (5).

From this, let the vectors which do not require other two phases' assistance to be defined as

—the independent vectors. Similarly, the vectors which require other phases' support are defined as

—the dependent vectors. According to these definitions,  $v_{100}$ ,  $v_{001}$ , and  $v_{010}$  are the independent vectors, while  $v_{111}$ ,  $v_{111}$ , and  $v_{111}$  are the dependent vectors in Fig. 5(b). Fig. 5(a) also compares the regions that can be composed by the independent. Here, the maximum amplitude of the phase voltage  $V_{ph\_max}$  in the linear modulation range is defined

$$V_{ph\_max} = V_m \left( V_{dc\_max} \frac{\sqrt{3}}{2} \right)$$

$$V_m = \left( \frac{4}{3} \underbrace{\frac{2 V_{dc\_max} - V_{dc\_mid}}{3}}_{\text{Voltage limitation from the medium dc link}} - \frac{2 V_{dc\_max} - V_{dc\_min}}{3} \right) \underbrace{\frac{1}{V_{dc\_max}}}_{\text{Voltage limitation from the minimum dc link}} \quad (6)$$

Where  $V_{dc\_max}$ ,  $V_{dc\_mid}$ , and  $V_{dc\_min}$  represent the maximum, medium, and minimum voltages among the dc links.

In fact, (6) can be simplified as

$$V_{ph\_max} = \frac{V_{dc\_mid} + V_{dc\_min}}{\sqrt{3}} \quad (7)$$

It should be noted that  $V_{ph\_max}$  is the maximum synthesizable voltage in the linear modulation range in the MLCI undergoing unbalanced dc-link conditions. From (7), it can be recognized that  $V_{ph\_max}$  is determined by  $V_{dc\_mid}$  and  $V_{dc\_min}$ . If all dc links are well balanced so that  $V_{dc\_mid}$  and  $V_{dc\_min}$  have identical values, (7) is rewritten as

$$V_{ph\_max} = \frac{2}{\sqrt{3}} V_{dc} \quad (8)$$

This is exactly double the maximum synthesizable voltage in the linear modulation range of a traditional three-phase half bridge inverter. In fact, the inverter in Fig. 4 is considered as a three-phase full-bridge inverter which is fed by independent dc links. To extend the proposed approach to the multistage MLCI using PS modulation, the total dc-link voltage per phase is represented as

$$V_{dc\_p} = \sum_{j=1}^N V_{dc\_p(j)} \quad p=a, b, or c \quad (9)$$

Where  $p$  represents a certain phase among phases  $a$ ,  $b$ , and  $c$ ,  $N$  is the number of the power stage modules in each phase, and  $j$  represents the index of a power stage module in each phase. In the multistage MLCI, (9) is utilized to obtain  $V_{dc\_max}$ ,

$V_{dc\_mid}$ , and  $V_{dc\_min}$ . After that, (7) is still applied.

### III. NUTRAL VOLTAGE MODULATION TECHNIQUE

In Section II, the maximum synthesizable voltage in the linear modulation range was evaluated under the unbalanced dc links. In this section, a method is proposed to realize the maximum modulation index in the linear modulation range under these conditions.

#### A. Traditional Offset Voltage Injection Method

The offset voltage injection scheme is a popular technique in three-phase half-bridge inverter applications. The theory behind this is that an offset voltage is incorporated with phase voltage

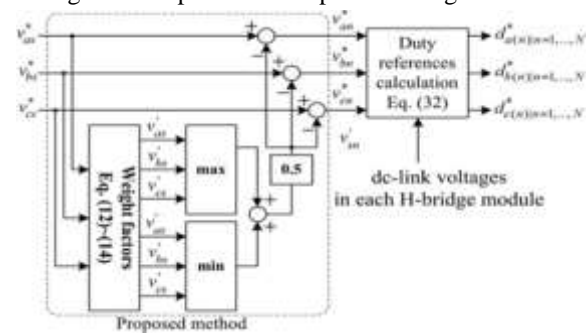


Fig. 6. Implementation of the NVM method

References to implement various PWM schemes in carrier-based PWM by using the fact that line-to-line voltage are applied to a three-phase load. For example, the offset voltage  $v^*_{sn}$  is injected to the phase voltage references  $v^*_{as}$ ,  $v^*_{bs}$ , and  $v^*_{cs}$  to implement carrier-based SVPWM as in

$$v^*_{sn} = \frac{v^*_{max} + v^*_{min}}{2} \quad v^*_{max} = \max(v^*_{as}, v^*_{bs}, v^*_{cs})$$

$$v^*_{min} = \min(v^*_{as}, v^*_{bs}, v^*_{cs}) \quad (10)$$

Then, the pole voltage references  $v^*_{an}$ ,  $v^*_{bn}$ , and  $v^*_{cn}$ , which will be converted to PWM duty references, are

$$v^*_{an} = v^*_{as} - v^*_{sn} \quad v^*_{bn} = v^*_{bs} - v^*_{sn} \quad v^*_{cn} = v^*_{cs} - v^*_{sn} \quad (11)$$

However, the aforementioned technique may not maximize the linear modulation range in MLCI undergoing unbalanced dc-link conditions.

#### B. Proposed NVM Method

If the dc links in an MLCI are unbalanced and the traditional offset voltage injection methods are utilized, the three-phase output voltages may become distorted as the phase voltage reference approaches  $V_{ph\_max}$ . This is because the traditional methods are not considering unbalanced dc-link conditions. Therefore, even if a phase can synthesize an output

voltage reference in the linear modulation range, the other phases can be saturated or go into the over modulation region. In this situation, a neutral voltage can be produced by the saturated or over modulated phase. In order to resolve this issue and to synthesize the output voltage to  $V_{ph\_max}$  in the linear modulation range, the NVM technique is proposed in this paper. Fig. 8 shows the concept of the proposed NVM technique. Here, a neutral voltage between the two neutral points  $n$  and  $s$  in Fig. 4 is modulated to compensate the output voltage imbalance caused by unbalanced dc-link conditions. To do this, first, the weight constant  $K_w$  is defined as

$$K_w = \frac{V_{dc\_mid} + V_{dc\_min}}{2} \quad (12)$$

By using (12), the weight factors are calculated as

$$K_{w\_a} = \frac{K_w}{V_{dc\_a}} \quad K_{w\_b} = \frac{K_w}{V_{dc\_b}} \quad K_{w\_c} = \frac{K_w}{V_{dc\_c}} \quad (13)$$

where  $K_{w\_a}$ ,  $K_{w\_b}$ , and  $K_{w\_c}$  represent the weight factors for phases a, b, and c, respectively. Next, the weight factors are multiplied by the phase voltage references, and the new references  $v_{as}$ ,  $v_{bs}$ , and  $v_{cs}$  are obtained as

$$v'_{as} = K_{w\_a} v_{as}^* \quad v'_{bs} = K_{w\_b} v_{bs}^* \quad v'_{cs} = K_{w\_c} v_{cs}^* \quad (14)$$

It should be noted that, depending on dc-link conditions, the sum of  $v_{as}$ ,  $v_{bs}$ , and  $v_{cs}$  may not be zero. By using these components, the injected voltage  $v_{sn}$  and the pole voltage References are given as

$$v'_{max} = \max(v'_{as}, v'_{bs}, v'_{cs}) \quad v'_{min} = \min(v'_{as}, v'_{bs}, v'_{cs})$$

$$v'_{sn} = \frac{v'_{max} + v'_{min}}{2} \quad \begin{bmatrix} v'_{an} \\ v'_{bn} \\ v'_{cn} \end{bmatrix} = \begin{bmatrix} v'_{as} - v'_{sn} \\ v'_{bs} - v'_{sn} \\ v'_{cs} - v'_{sn} \end{bmatrix} \quad (15)$$

From (15), the line-to-line voltages across each phase of the load are represented as

$$\begin{bmatrix} v_{ab}^* \\ v_{bc}^* \\ v_{ca}^* \end{bmatrix} = \begin{bmatrix} v_{an}^* - v_{bn}^* \\ v_{bn}^* - v_{cn}^* \\ v_{cn}^* - v_{an}^* \end{bmatrix} = \begin{bmatrix} v_{as}^* - v'_{sn} - v_{bs}^* + v'_{sn} \\ v_{bs}^* - v'_{sn} - v_{cs}^* + v'_{sn} \\ v_{cs}^* - v'_{sn} - v_{as}^* + v'_{sn} \end{bmatrix}$$

$$= \begin{bmatrix} v_{as}^* - v_{bs}^* \\ v_{bs}^* - v_{cs}^* \\ v_{cs}^* - v_{as}^* \end{bmatrix} \quad (16)$$

As it can be seen in (16),  $v_{sn}$  does not appear in the line-to-line voltages, and it is still considered as a hidden freedom of voltage modulation. Now, let us consider the role of the weight factors  $K_{w\_a}$ ,  $K_{w\_b}$ , and  $K_{w\_c}$ , which are inversely proportional to the corresponding dc-link voltage. For convenience, let us assume that the magnitudes of the dc-link voltage are under the following relationship:

$$V_{dc\_a} < V_{dc\_b} < V_{dc\_c} \quad (17)$$

Then, from (13) and (17)

$$K_{w\_a} > K_{w\_b} > K_{w\_c} \quad K_{w\_a} > 1$$

$$K_{w\_b}, K_{w\_c} < 1 \quad (18)$$

Equation (18) gives

$$|v'_{as}| > |v_{as}^*| \quad |v'_{bs}| < |v_{bs}^*| \quad |v'_{cs}| < |v_{cs}^*| \quad (19)$$

From (15) and (19), it can be recognized that, if  $v_{as}$ , whose dc-link voltage is less than the others, is corresponding to  $v_{max}$  or  $v_{min}$ , the absolute value of  $v_{sn}$  is greater than  $v_{sn}$  in (10).

On the other hand, the final pole voltage references  $v_{an}$ ,  $v_{bn}$ , and  $v_{cn}$  are calculated by subtracting  $v_{sn}$  from the original phase voltage references  $v_{as}$ ,  $v_{bs}$ , and  $v_{cs}$  as in (15). From this reasoning, in this example, it is supposed that, if  $v_{as}$  is corresponding to  $v_{max}$ , then the final pole voltage references  $v_{an}$ ,  $v_{bn}$ , and  $v_{cn}$  are less than the original pole voltage references Without  $v_{sn}$ .

1. Traditional carrier-based SVPWM.
2. Proposed NVM with  $V_{dc\_a} = 0.275 V_{dc}$ ,  $V_{dc\_b} = V_{dc}$ , and  $V_{dc\_c} = V_{dc}$ .
3. Proposed NVM with  $V_{dc\_a} = 0.2 V_{dc}$ ,  $V_{dc\_b} = V_{dc}$ , and  $V_{dc\_c} = V_{dc}$ . which are not considering  $v_{sn}$  but  $v_{sn}$ .

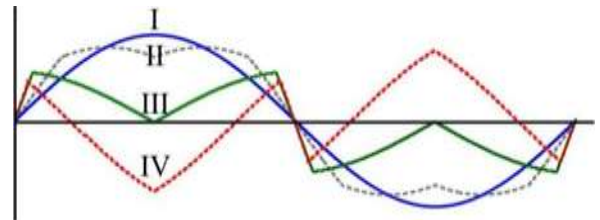


Fig.7. Comparison of modulated waveforms

On the contrary, if  $v_{cs}$  is  $v_{max}$ , then the final pole voltage references are greater than the original pole voltage references. By using this principle, the proposed method reduces the portion of the phase whose dc-link voltage is smaller than the others and increases the utilization of the phase in which the dc-link voltage is greater than those of the other phases. However, as it can be seen in (16),  $v_{sn}$  does not affect the line-to-line voltages. Therefore, the line-to-line voltage is the same as the one derived from the original phase voltage reference. From this analysis, the proposed method enables the maximum synthesizable modulation index in the linear modulation range under the unbalanced dc-link conditions to be achieved. In addition to this, if all of the dc-link voltages are well balanced so that  $V_{dc\_a}$ ,  $V_{dc\_b}$ , and  $V_{dc\_c}$  are equal to  $V_{dc}$

$$V_{dc\_mid} = V_{dc\_min} = V_{dc}. \quad (20)$$

By substituting (20) into (12)–(14)

$$K_w = \frac{V_{dc\_mid} + V_{dc\_min}}{2} = V_{dc}$$

$$K_{w\_a} = K_{w\_b} = K_{w\_c} = 1$$

$$v'_{as} = v^*_{as} \quad v'_{bs} = v^*_{bs} \quad v'_{cs} = v^*_{cs}. \quad (21)$$

Equation (21) shows that the proposed method gives the same voltage references as the traditional method under balanced dc-link conditions.

### C. Constraints of the Proposed Method

In this section, the limitation of how unbalanced dc links can be while still being compensated by the proposed method is evaluated. Fig. 9 shows the modulated voltage waveforms with different modulation methods and dc-link conditions. In the figure, cases I and II show the results of traditional sinusoidal PWM (SPWM) and carrier-based SVPWM, while cases III and IV illustrate the waveforms of the proposed method with different ratios of dc-link voltages. The fundamental idea to examine the limitation of the proposed method is to evaluate what conditions bring the different polarities between the original voltage reference and the modified voltage reference by using the proposed method. In Fig. 7, the vertices at  $\pi/2$  and  $3\pi/2$  rad almost come in contact with, but do not cross, the zero point. However, the directions of the vertices are opposite the original phase voltage reference in case IV. This means that an excessive and unnecessary voltage is injected into the system. As a result,

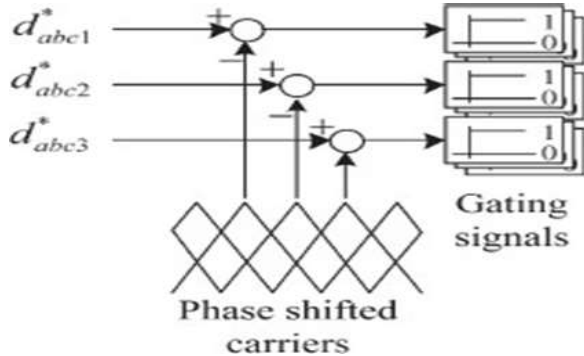


Fig.8. Comparison of the duty references and the carriers

The maximum linear modulation range is reduced, and the line to-line voltage may be distorted. With this basic concept, it is assumed that a phase which has the lowest dc-link voltage commands  $v^*_{max}$  and a phase which has the highest dc-link voltage

commands  $v^*_{min}$  to examine a worst case situation. From (14) and (15), the following equations can be established:

$$v'_{max} = \frac{V_{dc\_mid} + V_{dc\_min}}{2V_{dc\_min}} v^*_{max}$$

$$v'_{min} = \frac{V_{dc\_mid} + V_{dc\_min}}{2V_{dc\_max}} v^*_{min}$$

$$v'_{sn} = \frac{v'_{max} + v'_{min}}{2}. \quad (22)$$

By using (22), the pole voltage reference which is considered as the worst case is

$$v^*_{max\_n} = v^*_{max} - \frac{v'_{max} + v'_{min}}{2}. \quad (23)$$

By substituting (22) into (23), we have

$$v^*_{max\_n} = \left(1 - \frac{V_{dc\_mid} + V_{dc\_min}}{4V_{dc\_min}}\right) v^*_{max} - \frac{V_{dc\_mid} + V_{dc\_min}}{4V_{dc\_max}} v^*_{min}. \quad (24)$$

Fig.12. Simulation result of SPWM, three-phase voltage references are not zero simultaneously, near a positive peak of the original voltage reference, the sufficient condition which guarantees the same polarity between  $v^*_{max}$  and  $v^*_{min}$  is established as follows:

$$v^*_{max\_n} > 0 \quad v^*_{max} > 0 \quad v^*_{min} < 0. \quad (25)$$

By substituting (24) into the first condition in (25), the following condition can be written:

$$k_1 v^*_{max} > k_2 v^*_{min} \quad k_1 = 1 - \frac{V_{dc\_mid} + V_{dc\_min}}{4V_{dc\_min}}$$

$$k_2 = \frac{V_{dc\_mid} + V_{dc\_min}}{4V_{dc\_max}}. \quad (26)$$

Here, it is obvious that  $k_2$  is always positive. Therefore, as long as  $k_1$  is positive, the condition (26) is always satisfied, and  $k_1$  can be rearranged as follows:

$$k_1 = \left(\frac{3V_{dc\_min} - V_{dc\_mid}}{4V_{dc\_min}}\right). \quad (27)$$

Equation (28) is then directly obtained from (27) to ensure that  $k_1$  will always be positive

$$V_{dc\_min} > \frac{1}{3} V_{dc\_mid}. \quad (28)$$

Note that (28) is a sufficient condition to meet the conditions in (25) so that the proposed method can be applied. However, even if (28) is not satisfied so that  $k_1$  is negative, there still is a chance to apply the proposed method. To deal with this situation, let us consider the relationship between  $v^*_{max}$  and  $v^*_{min}$  as follows at a positive peak point:

$$v_{max}^* = -2v_{min}^* \tag{29}$$

By substituting (29) into (26), we have  $-2k_1 > k_2$ . (30)

Since  $k_1$  is negative in this case, the following condition is derived from (30);

$$|k_1| < \frac{k_2}{2} \tag{31}$$

If the relationship between  $k_1$  and  $k_2$  is established as in (31), even if the provision in (28) is broken, the conditions in (25) are satisfied so that the proposed method can be still effective. Let us recall Fig. 7 again here. In the figure, the values of  $|k_1|$  and  $k_2/2$  for case III are evaluated as 0.1591 and 0.1593, respectively. Although the difference between the two values is very small, (31) is still true with these values. For case IV, the values of  $|k_1|$  and  $k_2/2$  are calculated as 0.5 and 0.3, respectively. In contrast to case III, (31) is no longer satisfied, and the directions of the vertices are opposite, as explained previously. From the analysis in this section, both the methods in are successfully able to judge the availability of the proposed method. In terms of accuracy, the latter may give better results. However, in practice, the former may be useful to judge the operation of the proposed method because it is already dealing with an extremely worst case on its own and the calculation in real time is much simpler than (31).

**D. Duty Calculation**

The final voltage references are entered to the duty reference calculation block. In this block, the duty references of each H-bridge module are calculated as follows:

$$d_{a1}^* = d_{a2}^* = \dots = d_{aN}^* = \frac{v_{an}^*}{V_{dc\_a}}$$

$$d_{b1}^* = d_{b2}^* = \dots = d_{bN}^* = \frac{v_{bn}^*}{V_{dc\_b}}$$

$$d_{c1}^* = d_{c2}^* = \dots = d_{cN}^* = \frac{v_{cn}^*}{V_{dc\_c}} \tag{32}$$

The calculated duty references are compared to PS carriers to generate gating signals, as shown in Fig. 8. It should be noted that the duty references for each H-bridge in each phase are shared in the PS modulation.

**IV. SIMULATION MODEL OF PWM STAREGY BASED MULTILEVEL INVERTER**

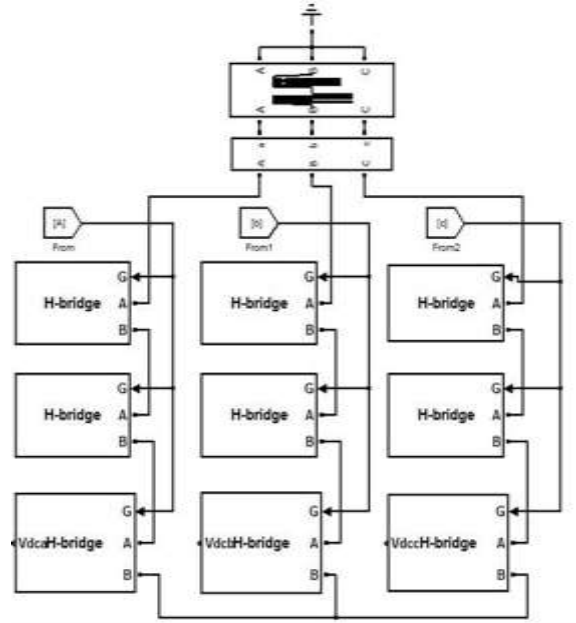


Fig.9.Simulink Model of Multilevel Cascaded Inverter

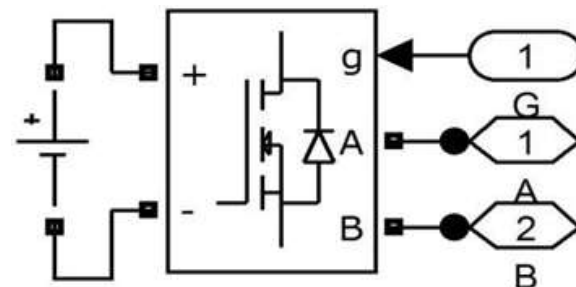


Fig.10. Cascade H-Bridge Inverter Module

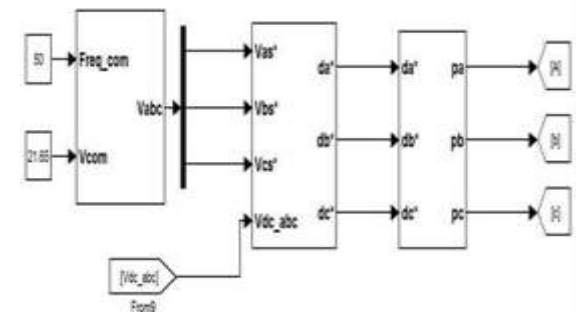


Fig.11.Control Module of Cascade Inverter

**V. SIMULATION RESITS OF MULTILEVEL CASCADED INVERTER**

**1. SPWM BASED INVERTER**

Simulation results of SPWM based multilevel cascaded inverter is as shown fig.12 and %THD of current and voltages as shown in fig.13 & fig.14.

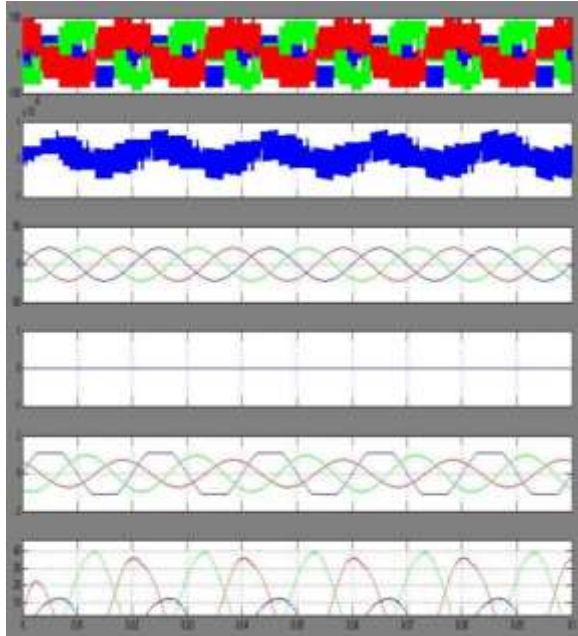


Fig.12. Simulation Result of Traditional SPWM

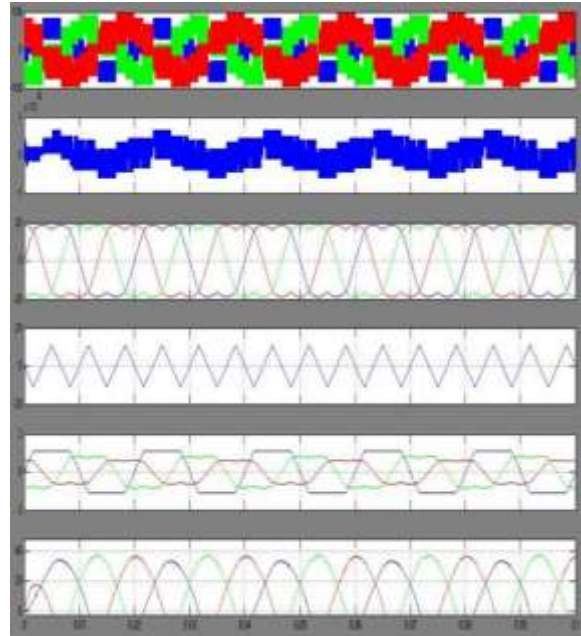


Fig.15. Simulation Result of Traditional SVPWM

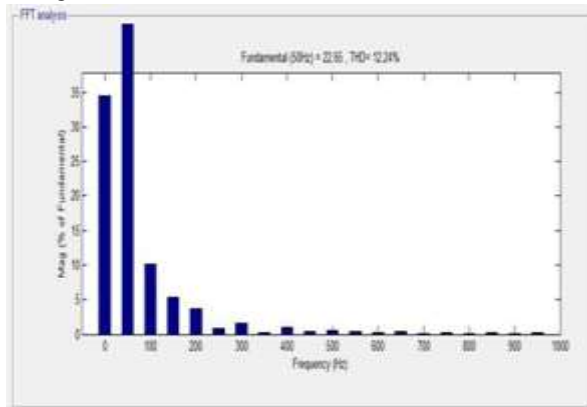


Fig.13. %THD at Output Current

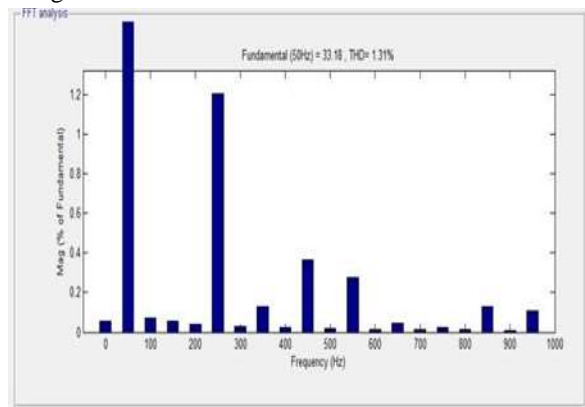


Fig.16. %THD at Output Current

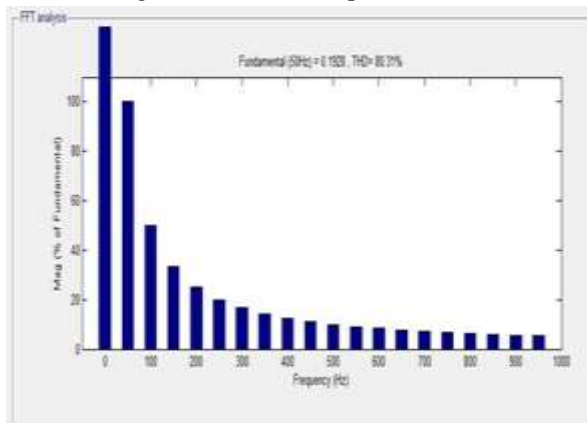


Fig.14. %THD at Output Voltage

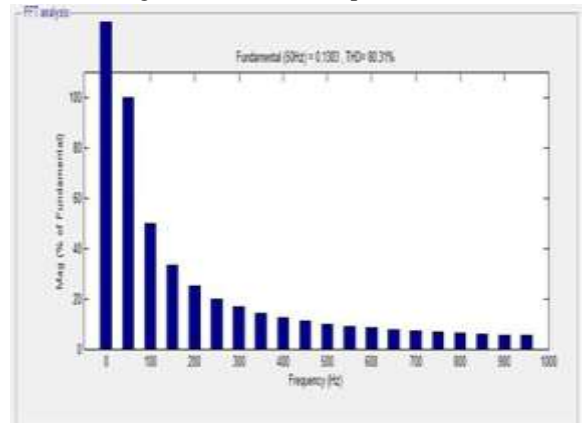


Fig.17. %THD at Output Voltage

## 2. SVPWM BASED INVERTER

Simulation results of SPWM based multilevel cascaded inverter is as shown fig.15 and %THD of current and voltages as shown in fig.16 & fig.17.

## 3. NVM BASED INVERTER

Simulation results of SPWM based multilevel cascaded inverter is as shown fig.18 and %THD of current and voltages as shown in fig.19 & fig.20



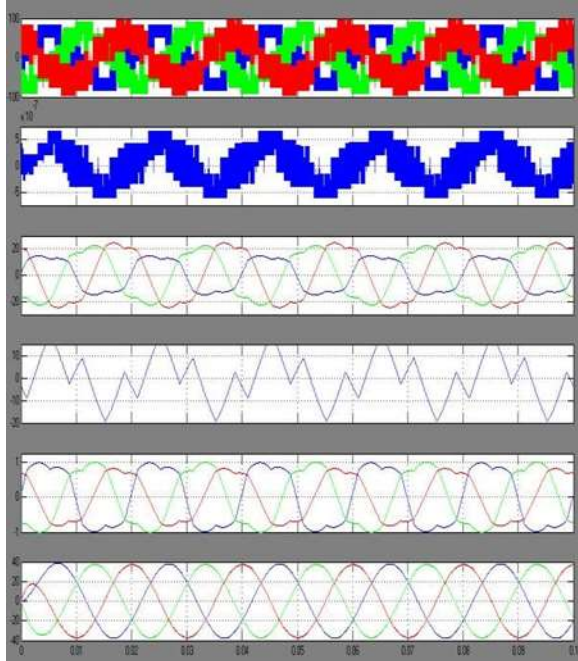


Fig.18. Simulation Result of Traditional NVM

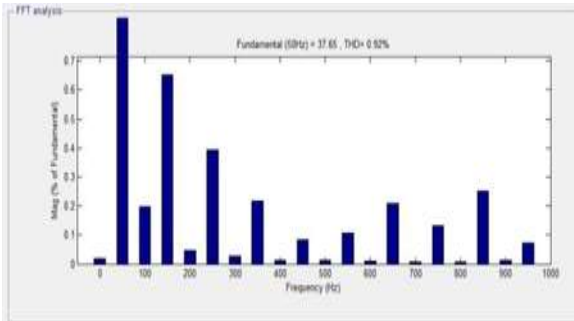


Fig.19. %THD at Output Current

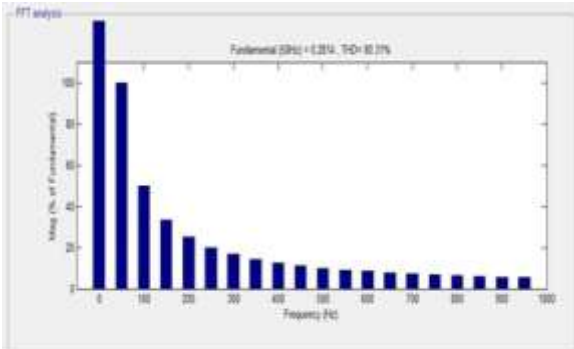


Fig.20. %THD at Output Voltage

### VI. PROPOSED PASSIVE LC FILTER BASED INVERTER

Passive LC filter is connected to compensate the harmonics present in inverter output voltage and current. We are placing LC filters with parameter values of  $L=20\text{mH}$  and  $C=0.5\text{F}$

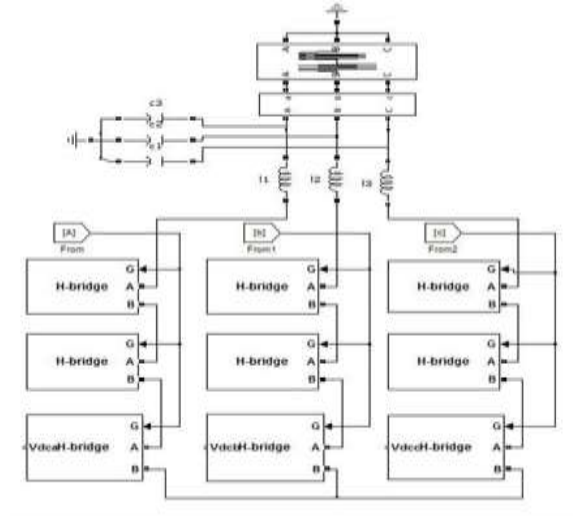


Fig.21. Simulink Model of Passive LC Filter Connected Inverter

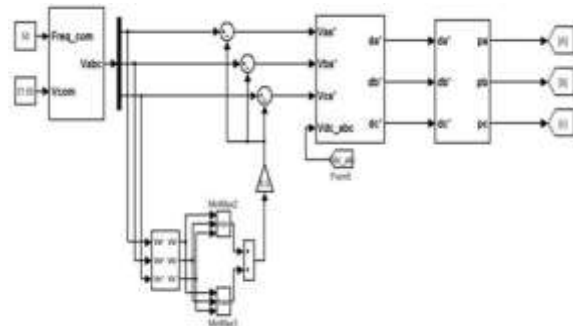


Fig.22. NVM Strategy Based Control System

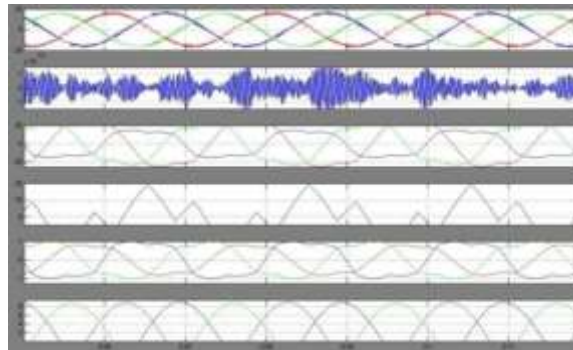


Fig.23. Simulation Result of NVM for LC Filter Based Inverter

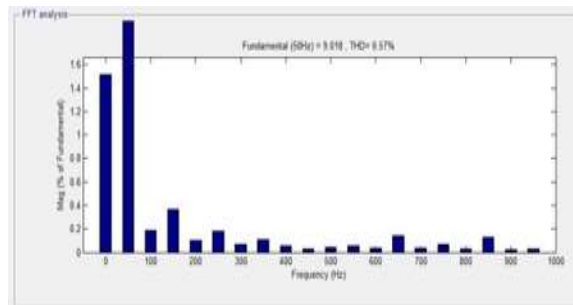


Fig.24. %THD at Output Current

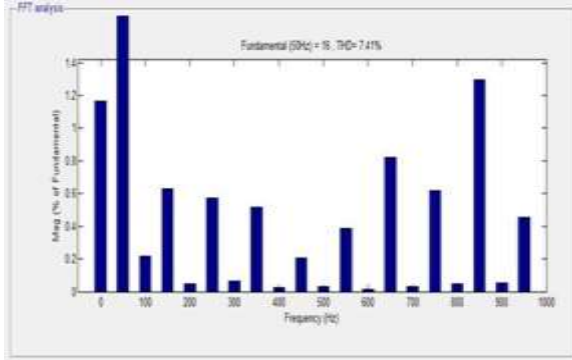


Fig.25. %THD at Output Voltage

TABLE I %THD COMPARISONS OF CONTROL STRATEGIES

	%THD IN CURRENT	%THD IN VOLTAGE
SPWM	12.24	80.31
SVPWM	1.31	80.31
NVM	0.92	80.31
LC FILTER BASED NVM	0.57	7.41

VII. CONCLUSION

The NVM technique for LC filter based MLCIs under unbalanced dc-link conditions have been proposed in this paper. In order to analyze the maximum synthesizable voltage of MLCIs, the voltage vector space has been analyzed using the switching function. From the analysis, the maximum linear modulation range was derived. The proposed NVM technique is applied to achieve the maximum modulation index in the linear modulation range under an unbalanced dc-link condition as well as to balance the output phase voltages and LC filter network reduces the harmonics present in inverter output voltage and currents. Compared to the previous methods, the proposed technique is easily implemented and improves the output voltage quality under unbalanced dc-link conditions. simulations results based on the IPM motor drive application verify the effectiveness of the proposed method.

REFERENCES

[1] J. Rodriguez, J.-S. Lai, and F. Z. Peng, Multilevel inverters: A survey of topologies, controls, and applications, *IEEE Trans. Ind. Electron.* vol. 49, no. 4, pp. 724–738, Aug. 2002.  
 [2] H. Abu-Rub, J. Holtz, J. Rodriguez, and G. Baoming, Medium-voltage multilevel

converters State of the art, challenges, and requirements in industrial applications, *IEEE Trans. Ind. Electron.*, vol. 57, no. 8, pp. 2581–2596, Aug. 2010.  
 [3] J.-S. Lai and F. Z. Peng, —Multilevel converters— A new breed of power converters, *IEEE Trans. Ind. Appl.*, vol. 32, no. 3, pp. 509–517, May/June. 1996.  
 [4] M. Malinowski, K. Gopakumar, J. Rodriguez, and M. A. Perez, —A survey on cascaded multilevel inverters, *IEEE Trans. Ind. Electron.*, vol. 57, no. 7, pp. 2197–2206, Jul. 2010.  
 [5] J. Rodriguez, L. G. Franquelo, S. Kouro, J. I. León, R. C. Portillo, M. A. M. Prats, and M. A. Perez, Multilevel converters: An enabling technology for high-power applications, *Proc. IEEE*, vol. 97, no. 11, pp. 1786–1817, Nov. 2009.  
 [6] G. Bergna, E. Berne, P. Egrot, P. Lefranc, A. Arzande, J.-C. Vannier, and M. Molinas, —An energy- based controller for HVDC modular multilevel converter in decoupled double synchronous reference frame for voltage oscillation reduction, *IEEE Trans. Ind. Electron.*, vol. 60, no. 6 pp. 2360–2371, Jun. 2013.  
 [7] Z. Shu, N. Ding, J. Chen, H. Zhu, and X. He, Multilevel SVPWM with DC-link capacitor voltage balancing control for diode-clamped multilevel converter based STATCOM, *IEEE Trans. Ind. Electron.*, vol. 60, no. 5, pp. 1884–1896, May 2013.  
 [8] J. Chavarria, D. Biel, F. Guinjoan, C. Meza, and J. J. Negroni, —Energy balance control of PV cascaded multilevel grid-connected inverters under level-shifted and phase-shifted PWMs, *IEEE Trans. Ind. Electron.*, grid-connected converter for renewable distributed systems, *IEEE Trans. Ind. Electron.*, vol. 60, no. 3, pp. 906–918, Mar. 2013.  
 [9] J. A. Munoz, J. R. R. Espinoza, C. R. Baier, L. L. Morán, E. E. Espinosa, P. E. Melín, and D. G. Sbarbaro, —Design of a discrete-time linear control strategy for a multicell UPQC, *IEEE Trans. Ind. Electron.*, vol. 59, no. 10, pp. 3797–3807, Oct. 2012.  
 [11] J. Napoles, J. I. Leon, R. Portillo, L. G. Franquelo, and M. A. Aguirre, —Selective harmonic mitigation technique for high-power

- converters,|| IEEE Trans. Ind. Electron., vol. 57, no. 7, pp. 2315– 2323, Jul. 2010.
- [10] L. G. Franquelo, J. Napoles, R. C. Portillo Guisado, J. I. Leon, and M. A. Aguirre, —A flexible selective harmonic mitigation technique to meet grid codes in three-level PWM converters,|| IEEE Trans. Ind. Electron., vol. 54, no. 6, pp. 3022–3029, Dec. 2007.
- [11] S. Kouro, M. Malinowski, K. Gopakumar, J. Pou, L. G. Franquelo, vol. 60, no. 1, pp. 98–111, Jan. 2013.
- [12] G. Buticchi, E. Lorenzani, and G. Franceschini, A five-level single-phase and B. Wu, —Recent advances and industrial applications of multilevel converters,|| IEEE Trans. Ind. Electron., vol. 57, no. 8, pp. 2553–2580 Aug. 2010.
- [13] A. M. Massoud, S. Ahmed, P. N. Enjeti, and B. W. Williams, —Evaluation of a multilevel cascaded- type dynamic voltage restorer employing discontinuous space vector modulation,|| IEEE Trans. Ind. Electron., vol. 57, no. 7, pp. 2398–2410, Jul. 2010.
- [14] M. Hagiwara, K. Nishimura, and H. Akagi, —A medium-voltage motor drive with a modular multilevel PWM inverter,|| IEEE Trans. Power Electron., vol. 25, no. 7, pp. 1786–1799, Jul. 2010.